

Three-Phase Flow in a Single-Strand Tundish During Start-Up Operation Using Top-Swirling Turbulence Inhibitor



JIAHUI WANG, QING FANG, LEI HUANG, PENG ZHAO, XUQI XIE,
and HUA ZHANG

A top-swirling turbulence inhibitor (TS-TI) was designed, and the three-phase behaviors of steel–slag–gas during the start-up operation with different TIs (without a TI, with an ordinary TI, with a TS-TI, and a TS-TI with different thickness of guide vanes) in a single-strand slab tundish were numerically and physically investigated and compared. The results showed that the molten steel exposed behaviors and residence time distribution (RTD) curves obtained by numerical simulations were consistent with the experiments. A swirling flow would be generated by using the designed TS-TI during start-up operation in the impact zone, thereby weakening the average velocity and level fluctuation of the steel–slag interface, and the steel exposure phenomenon at the whole filling process could be prevented when the thickness of guide vanes in the TS-TI was over 40 mm. After the molten steel level reached to steady-state level, exposed area of 1875 and 875 cm² for molten steel in the impact zone that without a TI and with an ordinary TI, respectively, and remains at 430 cm² when the guide vane thickness is 20 mm. Meanwhile, on applying the proposed TI, the time of slag adding operation could be 11.5 seconds earlier than that of an ordinary TI. Therefore, the TS-TI with the guide vane thickness around 40 mm could obviously improve the steel flow behavior, avoid steel exposure, and enhance the production efficiency of the single-strand tundish.

<https://doi.org/10.1007/s11663-022-02714-z>

© The Minerals, Metals & Materials Society and ASM International 2023

I. INTRODUCTION

AS an intermittent reaction vessel, the tundish not only ensures the continuous casting (CC) smoothly, but also has a remarkable influence on the internal and external quality of the final products.^[1–3] The start-up operation is the first stage in the working process of the tundish, which is one of the most polluting stage of the entire CC, including the secondary oxidation of molten steel, the injection of drainage sand, and suction.^[4–6] Before the start-up operation, the tundish is filled with argon gas to prevent secondary oxidation. However,

during the filling process, the air upon the top surface can be easily entrapped into the tundish due strong heat convection, and directly contact with the molten steel, by which cause serious secondary oxidation of molten steel. The secondary oxidation would be weakened after the slag film completely covers the molten steel. At the initial stage of start-up operation,^[7] the throughput in the ladle shroud (LS) is significantly greater than that of steady-state casting to ensure that the LS can be quickly submerged and minimize the three phases of steel–slag–gas mixing and gas suction in tundish. In the early stage of start-up operation, the stopper rod remains fully lowered, which is gradually lifted when the mass of molten steel accumulates to a certain value. During the stage, the protective slag is added to lower the heat loss of molten steel. Cwudziński *et al.*^[8] physically studied the time of molten steel mixing during the whole working period of tundish, and the optimal mixing conditions were determined. Braga *et al.*^[9] predicted the hydrogen pick-up of liquid steel during start-up operation by a mathematical model. Chakraborty *et al.*^[10] numerically simulated the heat transfer and movement of molten steel in tundish at the whole casting sequence and found that the main factor influencing the heat loss

JIAHUI WANG, QING FANG, PENG ZHAO, XUQI XIE, and HUA ZHANG are with the The State Key Laboratory of Refractories and Metallurgy, Wuhan University of Science and Technology, Wuhan 430081, P.R. China and also with the Key Laboratory for Ferrous Metallurgy and Resources Utilization of Ministry of Education, Wuhan University of Science and Technology, Wuhan 430081, P.R. China. Contact e-mail: qingfang@wust.edu.cn; huazhang@wust.edu.cn LEI HUANG is with the Guangxi Beigang New Material Co., Ltd., Beihai 536000, P.R. China.

Manuscript submitted August 1, 2022; accepted December 17, 2022.

Article published online January 5, 2023.

in tundish is the steel flow pattern and heat transfer characteristics, rather than the molten steel residence time in tundish.

The slag film plays an essential role in preventing heat loss and reoxidation of molten steel in the tundish. By analyzing the flow of slag, the phenomenon of molten steel exposure can be effectively weakened. At the same time, the appropriate timing of slag adding can improve production efficiency. Zhang *et al.*^[11] and Morales *et al.*^[12,13] numerically studied the steel-gas two-phase flow behaviors in the tundish under three different TIs during the filling process. However, the study only considers the steel-gas two phases in the tundish, and the behavior of the slag during the start-up operation was ignored. The main reason is that it is difficult to accurately simulate the slag adding during the start-up operation and the initial movement after the slag adding. In this study, a method for simulating slag adding during the start-up operation of the tundish was proposed.

The flow control device that has the greatest influence during the tundish filling is the turbulence inhibitor (TI). It can not only prevent the corrosion of the tundish lining but also reduce the liquid level fluctuation and promote the floating of inclusions.^[14] Morales *et al.*^[15] found that the TI could improve the fluid flow characteristics with the increase in the volume of plug zone, longer residence time. Studies References 16 through 18 showed that a reasonable swirling flow is beneficial to improve cleanliness of molten steel, promote the collision growth, and enhance the floating removal rate of non-metallic inclusions. However, the existing technology has the problems of complicated equipment installation, difficult to control the improvement effect and huge cost. A TS-TI with guide vanes inside was designed by Zhang *et al.*,^[11] the fluid flow and RTD curves and multiphase flow behavior under the TS-TI were numerically investigated, which showed apparent advantages on improving the steel cleanness. However, the numerical models were not directly verified and the slag behaviors during start-up operation were ignored.

In this paper, the flow behaviors of steel–slag–gas phases during start-up operation of a single-strand tundish without a TI, with an ordinary TI, and a TS-TI with different guide vane thickness were numerically investigated and discussed. The numerical results of RTD curves and steel exposure were validated by water model experiments. The present work not only provides ideas for simulating flow of steel–slag–gas during start-up operation but also offers theoretical guidance for further application and popularization of the present TS-TI.

II. MATHEMATICAL MODEL

A. Assumptions

The basic assumptions for complex turbulence and steel–slag–gas flow during the start-up operation were set as follows:

- (1) Ignoring the velocity changes of LS and submerged entry nozzle (SEN) during start-up operation;
- (2) The phases of steel, slag, and gas (air) in the simulation are considered to be incompressible Newtonian fluids;
- (3) The slag is poured into the tundish in a liquid state;
- (4) Ignoring the effect of temperature changes and inclusion on fluid flow in the tundish.

B. Basic Equations

1. Turbulent model

Turbulent behavior of molten steel is a complex process during start-up operation and the standard k - ε model is applied in this paper.^[19,20]

Turbulent kinetic energy (TKE) k :

$$\frac{\partial(\rho_m k)}{\partial t} + \nabla \cdot (\rho_m \vec{v}_m k) = \nabla \cdot \left[\left(\mu + \frac{\mu_{t,m}}{\sigma_k} \right) \nabla k \right] + G_k - \rho_m \varepsilon. \quad [1]$$

Turbulent dissipation rate ε :

$$\frac{\partial(\rho_m \varepsilon)}{\partial t} + \nabla \cdot (\rho_m \vec{v}_m \varepsilon) = \nabla \cdot \left[\left(\mu + \frac{\mu_{t,m}}{\sigma_k} \right) \nabla \varepsilon \right] + C_{1\varepsilon} \frac{\varepsilon}{k} G_k - C_{2\varepsilon} \rho_m \frac{\varepsilon^2}{k}, \quad [2]$$

where \vec{v}_m stands for mixture velocity, ρ_m stands for density, G_k stands for the generation of TKE by the mean velocity gradients, and μ stands for the laminar viscosity. The turbulent viscosity $\mu_{t,m}$ is calculated as

$$\mu_{t,m} = \rho_m c_\mu k^2 / \varepsilon, \quad [3]$$

where $C_{1\varepsilon} = 1.43$, $C_{2\varepsilon} = 1.92$, $c_\mu = 0.09$, $\sigma_k = 1.0$, and $\sigma_\varepsilon = 1.3$.

2. Multiphase model

To accurately expressed the behavior of multiphase flow in the tundish during start-up operation, the volume of fluid (VOF) model is used in this study.

Continuity equation:

$$\frac{1}{\rho_i} \left[\frac{\partial}{\partial t} (\alpha_i \rho_i) + \nabla \cdot (\alpha_i \rho_i \vec{v}_m) \right] = S_{\alpha_i} + \sum_{i=1}^n \left(m_{ji}^- - m_{ij}^- \right), \quad [4]$$

where m_{ji}^- and m_{ij}^- stand for the mass flow from phase i to phase j and phase j to phase i , respectively.

Momentum equation:

$$\frac{\partial(\rho_m \vec{v}_m)}{\partial t} + \nabla \cdot (\rho_m \vec{v}_m \vec{v}_m) = -\nabla P + \nabla \cdot [\mu_m (\nabla \vec{v}_m + \nabla \vec{v}_m^T)] + \rho_m \vec{g} + \vec{F}. \quad [5]$$

The physical parameters are calculated by the weighted average method, such as

$$\rho_m = \sum_{i=1}^3 \alpha_i \rho_i. \quad [6]$$

The surface tension force (\vec{F}) is calculated as follows:

$$\vec{F} = \sum_{\text{parisij}, i < j}^3 2\sigma_{ij} \frac{\alpha_i \rho_i k_j \nabla \alpha_j + \alpha_j \rho_j k_i \nabla \alpha_i}{\rho_i + \rho_j}, \quad [7]$$

where k_j and k_i are the radiuses of curvature; σ_i and σ_j stand for the surface tension of phase i and phases j , respectively; $\sigma_{ij} = \left(\sigma_i^2 + \sigma_j^2 - 2\sigma_i \sigma_j \cos \theta \right)^{\frac{1}{2}}$ is interfacial tension; θ stands for the contact angle between phases.

C. Initial and Boundary Conditions

According to the flow rate in the LS, the start-up operation is divided into four stages. Figure 1 shows the variation of tundish steel weight and LS throughput during start-up operation in the tundish with filling time. The first and second stages of the LS were injected at $3Q_{steady}$ (Q_{steady} is the flow rate of steady-state) to reach the start-up tonnage as soon as possible. The phenomena of concern at this stage include spreading/initial flow, air entrainment and gas absorption, temperature drop and strand freezing, etc. The LS was injected at $2Q_{steady}$ during the third stage and the phenomenon of concern at this stage is steel exposure. In the fourth stage, tundish tonnage reaches a steady-state level.

The boundary conditions of numerical simulation during start-up operation were set as follows:

- (1) The velocity inlet boundary was set for the inlet of LS, and the velocity $V_{in-steady} = 1.19$ m/s during steady-state casting. During the start-up operation, the inlet velocity $V_{in} = 3.57$ m/s at the first and second stages, which was $V_{in} = 2.38$ m/s at third stage;
- (2) The velocity inlet boundary was set for the outlet of SEN, and direction was $Z = -1$ after reaching the start-up operation tonnage. The average exit veloc-

ity was $V_{outlet} = 1.728$ m/s in order to simplify the calculations;

- (3) The boundary conditions for the slag entrances were set to be pressure-outlet before slag adding and after slag adding, while the boundaries were set to be velocity inlet during the slag adding process;
- (4) The boundary conditions for the upper wall were pressure-outlet, the material entering and leaving was gas.

D. Computational Procedure

The mesh of the tundish, the structure diagram of a TS-TI, and the parameters of a TS-TI are shown in Figure 2. The calculation model used the hexahedral structure mesh and the technology of local grid refinement was employed, the cells in the computed field were about 2,000,000. Moreover, the key industrial parameters of the single-strand tundish applied in the computations are listed in Table I.

Table II shows the physical parameters of the fluids in tundish. In the calculations, the thermophysical parameters of molten steel could be regarded as constants.

In this paper, the pressure implicit with splitting of operators (PISO) method was applied to couple the pressure and velocity terms, and the computation fluid dynamic commercial software ANSYS Fluent^[19] was used to calculate the three-dimensional flow field of the tundish. When calculating the multiphase flow, the explicit VOF model was used, the primary phase is molten steel, and the secondary phases are gas and slag.

III. MODEL VALIDATIONS

To validate the simulated results of multiphase flow behavior in the tundish, water model experiments were conducted based on the principle of similitude. Taking into account the flow of the LS and the conditions of the laboratory, the ratio of the experimental model in this study was 1:4 ($\lambda = 1/4$) compared with the prototype tundish. The molten steel and slag were modeled by water and a mixture of kerosene and vacuum pump oil, respectively.^[21] In this study, the case without a TI was named Case A, with an ordinary TI was named Case B, and with a TS-TI was named Case C.

The ratio of velocity, throughput, and time between the prototype tundish and water model could be determined through the equality of Froude number (Fr):

$$Fr_p = Fr_m, \quad \frac{v_p^2}{gL_p} = \frac{v_m^2}{gL_m}, \quad [8]$$

p stands for prototype and m stands for model; v , L , and g are flow velocity, characteristic length, and gravitational acceleration, respectively. Then, the LS injection flow rate $Q_m = \lambda^{\frac{5}{2}} Q_p$ and $v_m = \sqrt{\lambda} v_p$ can be calculated in the water model. The flow states and interactions between molten steel and slag are principally influenced by the surface tension in the tundish,

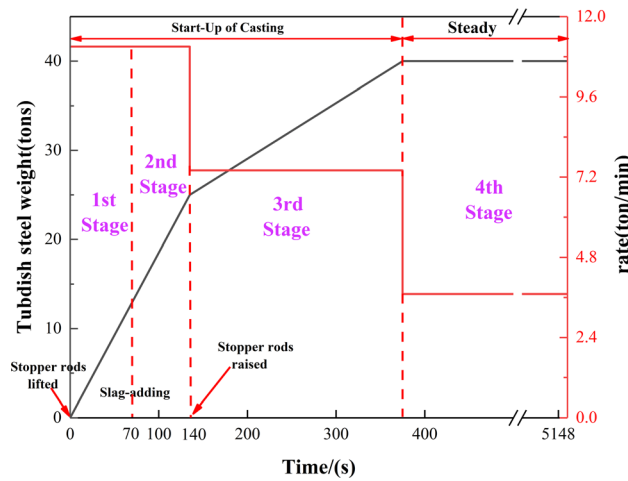


Fig. 1—The variation of steel weight and LS rate during start-up operation in the tundish.

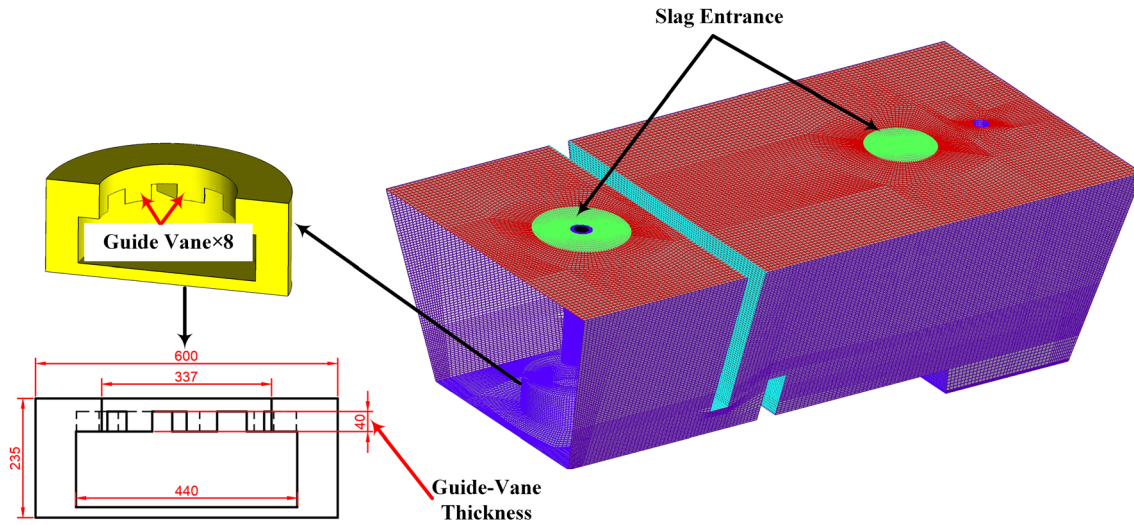


Fig. 2—The mesh of the tundish, the structure diagram of a top-swirling TI, and the parameters of a top-swirling TI (mm).

Table I. Key Parameters of the Tundish Applied in the Calculations

Industrial Parameters	Values
Tundish Tonnage at Steady-State(t)	40
Slab Size (mm ²)	2200 × 200
Typical Casting Speed (m/min)	1.15
Steel-Level Height at Steady-State Casting (mm)	965
LS Internal Diameter (mm)	95
SEN Internal Diameter (mm)	70
Start-Up Operation Tonnage (t)	25
Thickness of Liquid Slag Layer (mm)	40

Table II. Physical Parameters of Liquids in Calculations

Substance	Steel	Slag	Gas (Air)
Density (kg/m ³)	7200	2700	1.225
Viscosity (Pa s)	0.0062	0.2	1.79 × 10 ⁻⁵

so it should be ensured that the model and the prototype tundish have the same Weber number (We).^[22]

$$We_m = We_p \quad [9]$$

$$\frac{v_{\text{water}}^2 \rho_{\text{water}}}{[\sigma_{\text{water-oil}} g (\rho_{\text{water}} - \rho_{\text{oil}})]^{\frac{1}{2}}} = \frac{v_{\text{steel}}^2 \rho_{\text{steel}}}{[\sigma_{\text{steel-slag}} g (\rho_{\text{steel}} - \rho_{\text{slag}})]^{\frac{1}{2}}}, \quad [10]$$

where $\sigma_{\text{steel-slag}} = 1.6$, $\sigma_{\text{water-oil}} = 7.3 \times 10^{-3}$. Then the density of ρ_{oil} can be calculated:

$$\rho_{\text{oil}} = \rho_{\text{water}} - \frac{v_{\text{water}}^4 \cdot \rho_{\text{water}}^2 \cdot \sigma_{\text{steel-slag}}^2 (\rho_{\text{steel}} - \rho_{\text{slag}})}{v_{\text{steel}}^4 \cdot \rho_{\text{steel}}^2 \cdot \sigma_{\text{water-oil}}^2}. \quad [11]$$

Therefore, the volume ratio of vacuum pump oil and kerosene can be calculated to be 36:64.

Figure 3 shows the ruptures of the slag layer in numerical simulations and oil layer in experiments in the impact zone as the tundish filling time are 200, 220, 240 seconds, respectively, when different TIs were used. In Case A, the exposed position in the calculations and experiment were at the corners of the tundish wall. The exposed position of steel in Case B was near the LS, and in Case C would not cause steel exposure. At the same time, there was no obvious difference in the exposed shape of steel by comparing the numerical simulation and water model experiment in each case.

Table III presents the molten steel exposed area on the free surface of impact zone in the water model experiment (scaled up by similarity principle) and numerical simulation. In Case A, when the filling time was 200, 220, and 240 seconds, the exposed areas of water in water model experiments were 1976, 1926, and 1958 cm², respectively, and the steel-exposed areas in numerical simulations were 1913, 1880, and 1933 cm², respectively. The errors of exposed area were 3.29, 2.45, and 1.29 pct, respectively. In Case B, the errors of exposed area were 4.11, 3.56, and 5.82 pct, respectively, and the exposed area was zero in Case C. The results showed that the TS-TI can restrain the phenomenon of molten steel exposure, inhibit the reoxidation of molten steel, and improve the steel cleanliness.

Besides, when evaluating the advantage of a proposed TI, the investigation of the flow field at steady-state casting is inevitable. Zhang *et al.*^[11] had proved that the TS-TI showed no negative effect on the steady-state casting by numerical simulation without direct validation. To ensure the simulation accuracy, water experiments were also conducted to validate the results of RTD curves under different cases. After the flow field was stable, the tracer of 20 pct KCl solution was injected into the tundish through LS within 1.0 seconds, and the concentration change at the outlet was monitored and calculated to draw the RTD curves. The comparison of

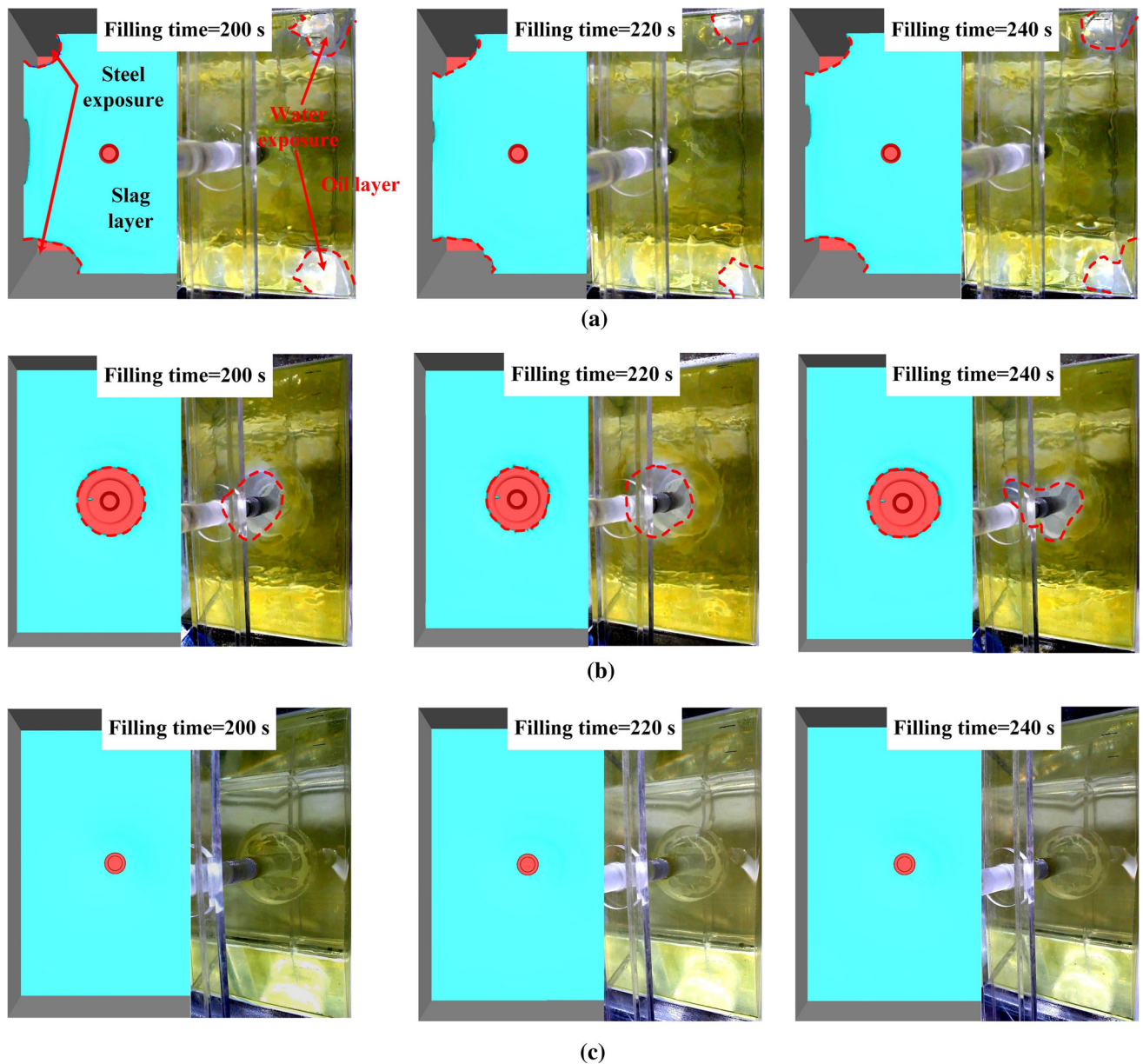


Fig. 3—Simulations and experiments of molten steel exposure at different times: (a) Case A; (b) Case B; (c) Case C.

RTD curves of numerical simulations and water model experiments under different TIs are shown in Figure 4 shows. Table IV shows the comparison and error of the average residence time obtained by the two simulation methods. The error of average residence time of molten steel obtained by the two simulation methods was less than 8 pct. Compared with Case A, the average residence time of Case B and Case C would be prolonged by about 50 seconds, which was conducive to the floating of inclusions in molten steel. At the same time, since there was no TI in Case A, the molten steel flows directly to SEN after flowing into the impact zone from the LS, resulting in short-circuit flow.

By above, the VOF model can accurately predict the steel-slag-gas flow behavior, and the RTD curves between the experiments and simulations basically match.

IV. RESULTS AND DISCUSSIONS

A. Steel Turbulent Flow

Figure 5 shows the velocity contours and vectors of the steel-slag interface at the impact zone under different TIs at filling time are 90, 110, 130 seconds, respectively. Table V lists the average velocity in each

Table III. Comparison Between Simulations and Experiments of Molten Steel Exposure

Case	Case A			Case B			Case C		
Time (s)	200	220	240	200	220	240	200	220	240
Experiments $\times 16$ (cm ²)	1976	1926	1958	887	901	927	0	0	0
Simulations (cm ²)	1913	1880	1933	852	870	876	0	0	0
Errors (Pct)	3.29	2.45	1.29	4.11	3.56	5.82	0	0	0

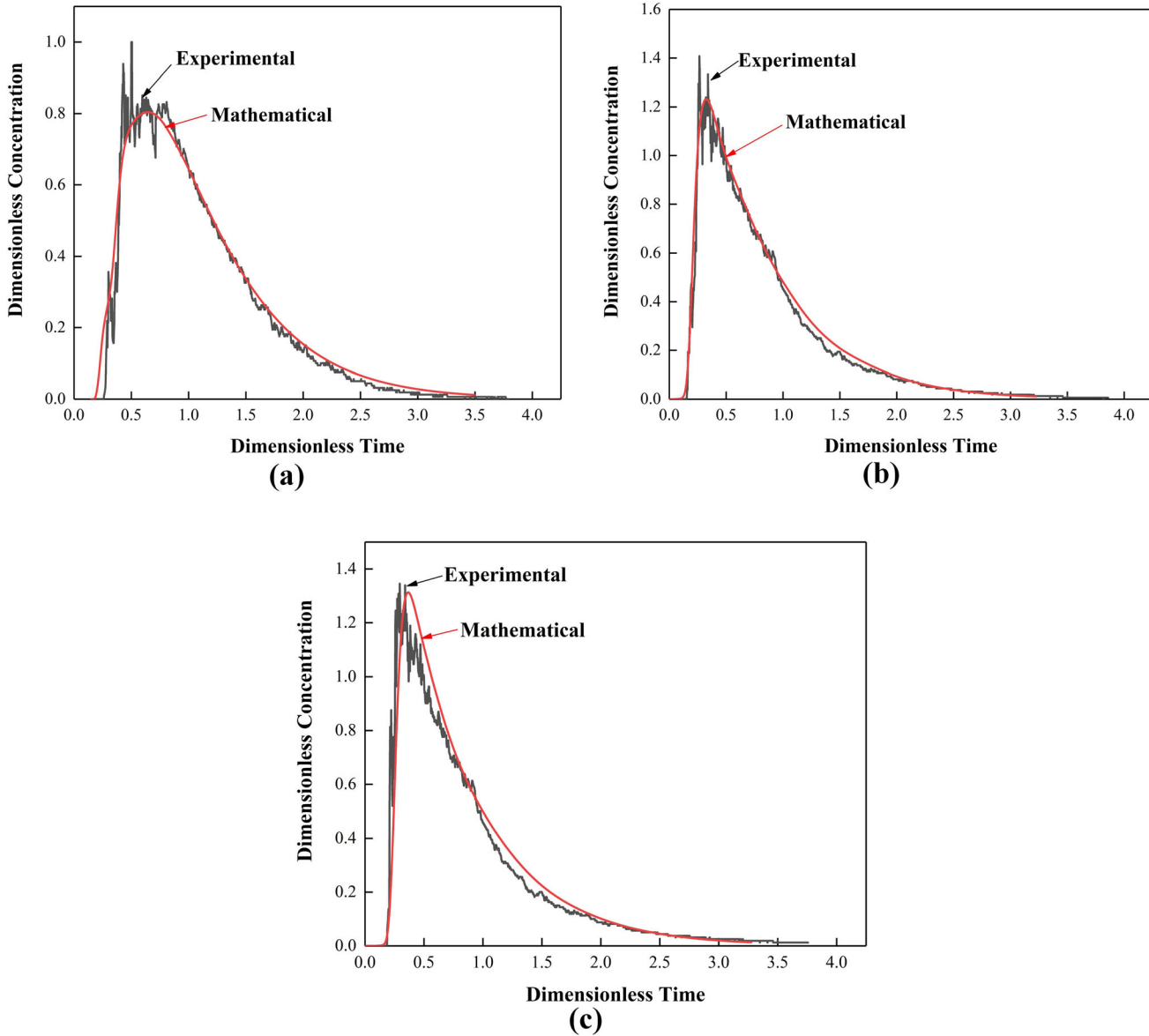


Fig. 4—The RTD curves between numerical simulations and water model experiments: (a) Case A; (b) Case B; (c) Case C.

interface. It can be seen that the free surface gradually rises and the average velocity gradually decreases as the filling progresses. The average velocity of the Case C at each moment of filling was apparently smaller than Case B. In Case B, the molten steel average velocity on the steel–slag interface was 0.079, 0.075, 0.065 m/s at 90, 110, 130 seconds, respectively, which was reduced by 29.11, 49.33, and 43.08 pct in Case C. Because of the obvious rotational flow field could be generated in Case

C, part of the steel TKE could be transformed into the horizontal swirling potential energy. This is conducive to reducing the TKE of molten steel returning to the steel–slag interface, thereby reducing the fluctuation of free surface and preventing secondary oxidation.

During start-up operation, the liquid level fluctuates greatly due to the low liquid level. At this time, slag adding will cause a large amount of slag entrainment. Therefore, the slag should be added when the tundish

liquid level fluctuation is relatively small. In this study, when the liquid level reached 300 mm (that is, the tundish starts filling for 70 seconds), the bottom of LS was already submerged into the molten steel, so the operation of covering slag adding was carried out. Figure 6 shows the variation of free surface fluctuation at the filling time is 50, 60, and 70 seconds, respectively. Figure 7 shows the liquid level waveforms diagram of X-axial section during the start-up operation. Figures 6 and 7 show that in Case B, before slag adding, the liquid

level fluctuation was relatively severe since the inlet flow rate was $3Q_{steady}$ and the molten steel level was lower. As the liquid level rises, the liquid level fluctuation gradually weakens. When filling time was 50, 60, and 70 seconds, the fluctuation of the molten steel was 85, 52, and 40 mm in Case B, respectively, which was 54, 35, and 23 mm in Case C. The fluctuation in Case C at each stage was weaker than Case B. It shows that the TS-TI can effectively weaken the free surface fluctuation. In Case B, the fluctuation was reduced from 120 mm at 40 seconds to 40 mm at 70 seconds. The fluctuation of the final molten steel level would be stable at about 30 mm,^[11] so it is reasonable to choose this time as the slag addition time.

The liquid level fluctuation of the tundish with different cases before slag adding is shown in Figure 8. Figure 8 shows that in Case B, after the tundish was filled for 70 seconds, that is, when the weight of molten steel in tundish reaches the slag adding tonnage, the

Table IV. The Average Residence Time Error of Water Model Experiment and Numerical Model Calculation

Case	Case A	Case B	Case C
Experimental $\times 2$ (s)	617.1	677.4	654.8
Mathematical (s)	654.4	707.3	707.7
Errors (Pct)	5.70	4.23	7.47

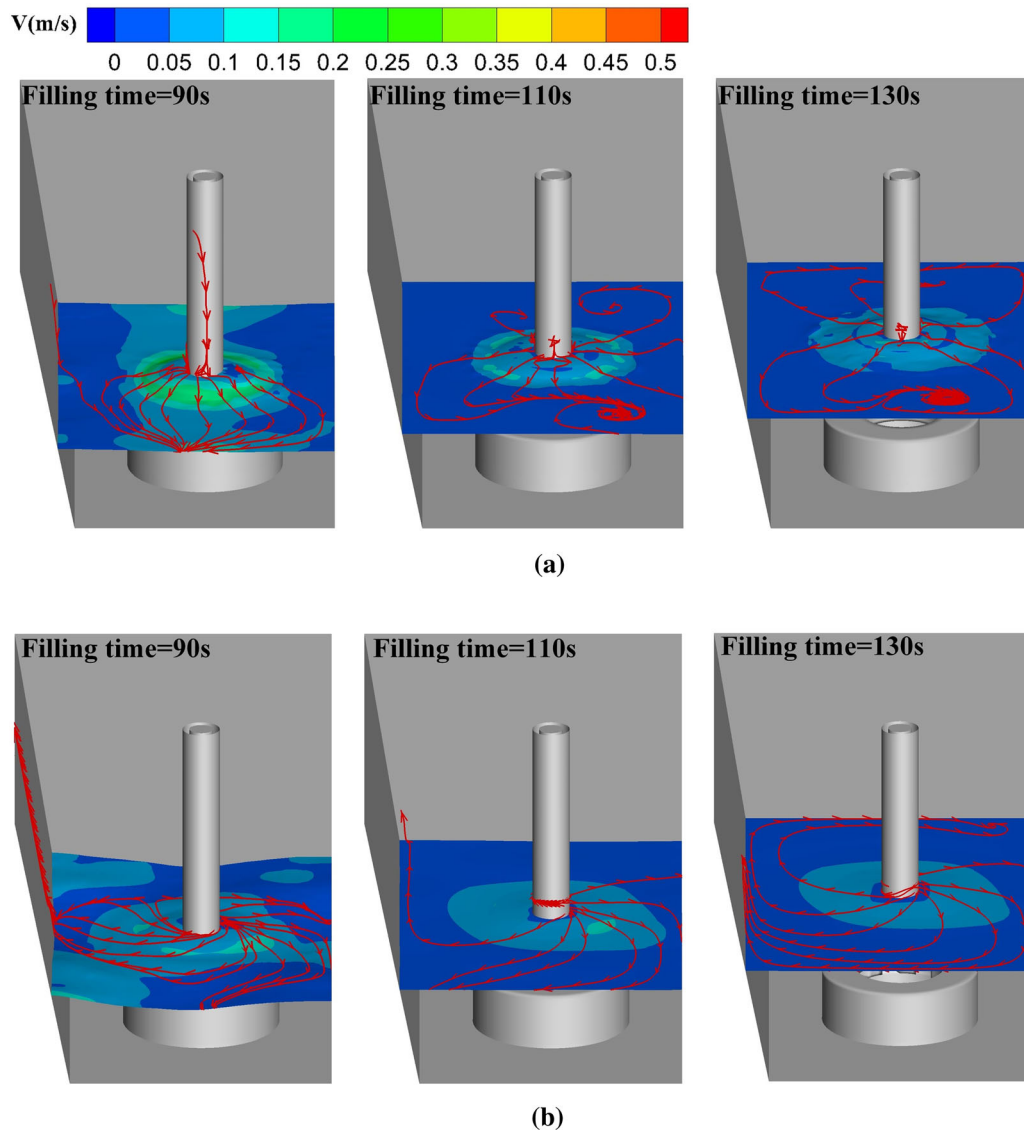


Fig. 5—Velocity contours at the steel–slag interface during start-up operation at filling time is 90, 110, and 130 s: (a) Case B; (b) Case C.

Table V. The Average Velocity of the Location and Filling Time Corresponding to the Steel–Slag Interface in Fig. 5

Filling Time (s)	Case B, (m/s)	Case C (m/s)	Reduction Rate (Pct)
90	0.079	0.056	29.11
110	0.075	0.038	49.33
130	0.065	0.037	43.08

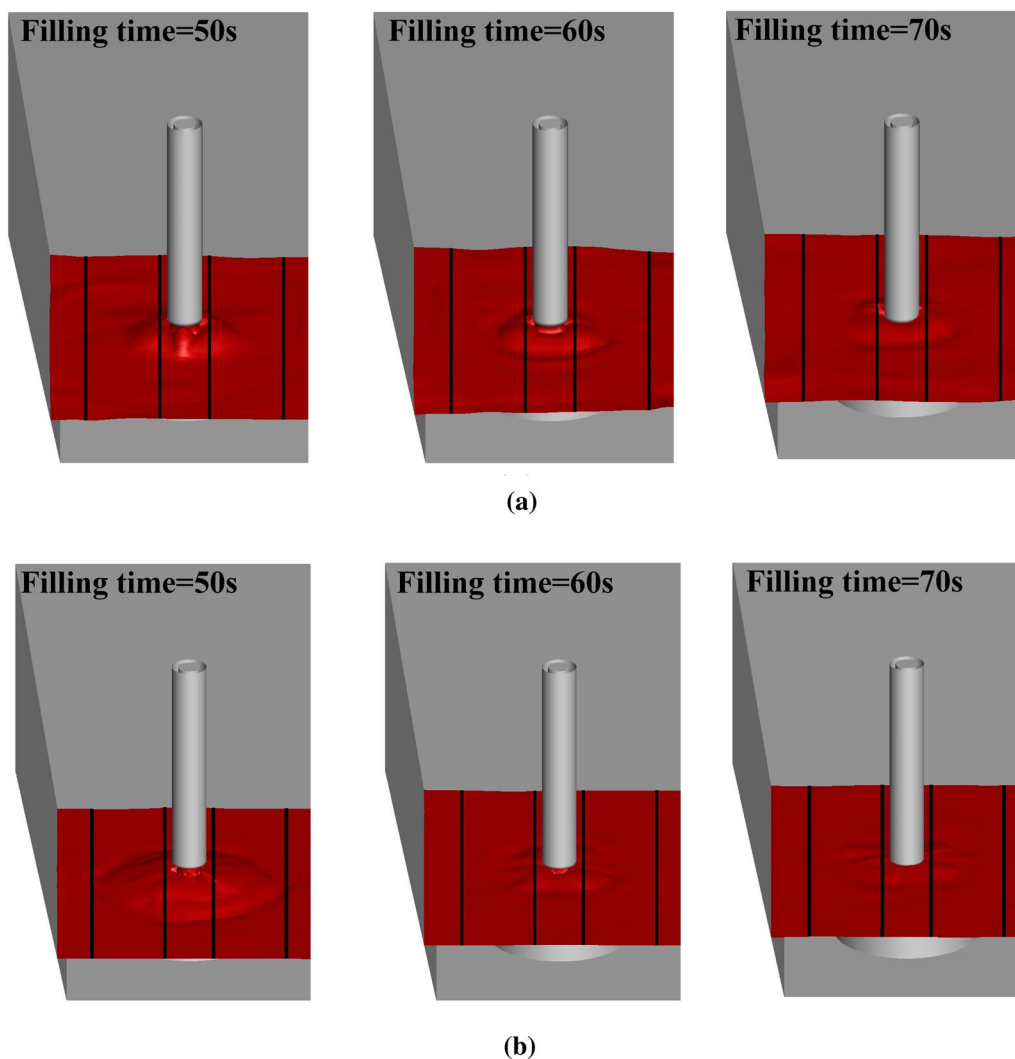


Fig. 6—The fluctuation of the free surface at filling time is 50, 60, 70 s: (a) Case B; (b) Case C.

liquid level fluctuation was 40 mm. In Case C, the liquid level fluctuation of 40 mm corresponded to the filling time of about 58.5 seconds. It shows that the slag adding operation of Case C can be carried out at least 11.5 seconds earlier than Case B. Before slag adding, the reoxidation of the molten steel is extremely serious because the air is in direct contact with the molten steel. In actual production, the molten steel is seriously polluted during this period, so the slag addition operation in advance can improve the production efficiency and improve the metal yield. At the same time, compared with Case B, Case C can significantly reduce the fluctuation of the liquid level, it is beneficial to

reduce the probability of slag entrainment and reoxidation, and improve the steel cleanliness, reducing the scrap rate of head billet.

B. Slag Phase

Figure 9 shows the flow of slag under different cases during the start-up operation. Case A and Case B had different degrees of slag entrainment into the molten steel when the slag was added, and basically no slag entrainment into the molten steel under Case C. At the same time, Case B is far less than Case A for the slag entrainment into molten steel. In Case A, the floating

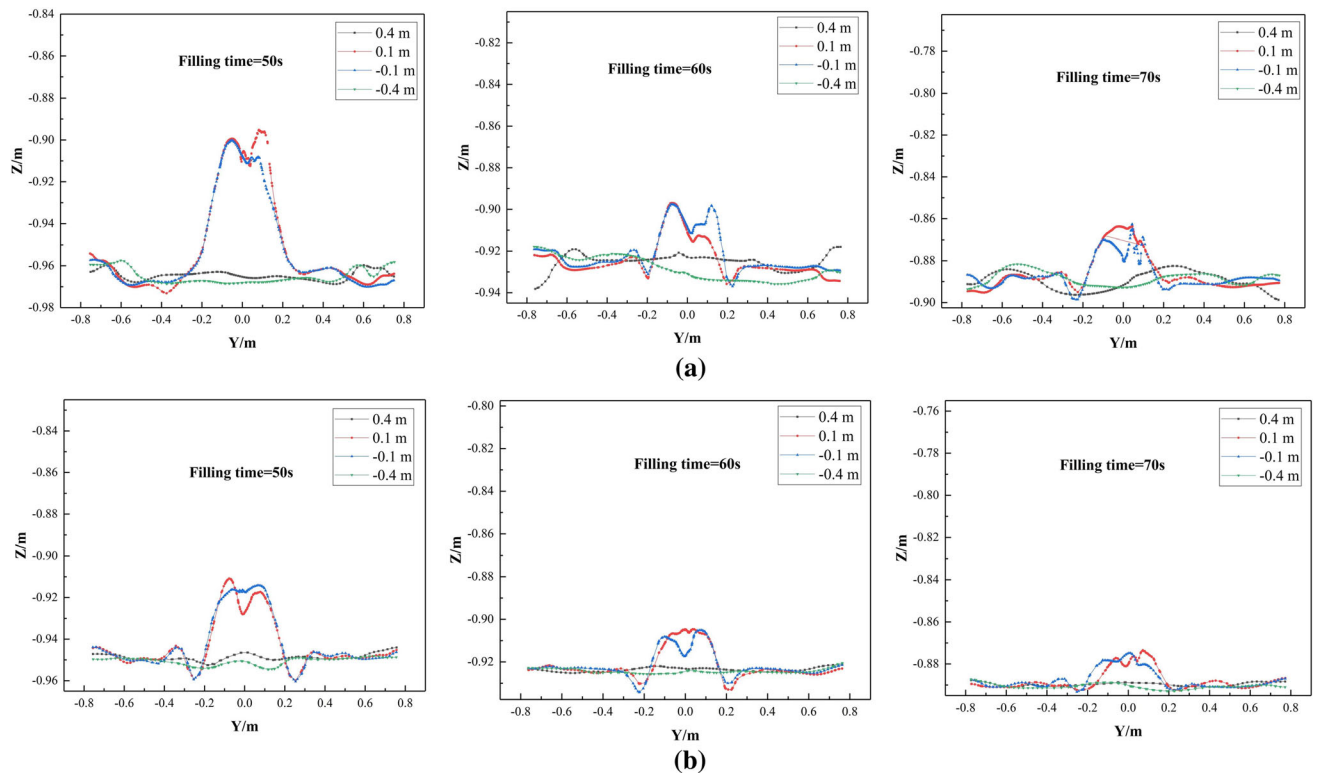


Fig. 7—The waveforms diagram of X-axial section at filling is 50, 60, 70 s: (a) Case B; (b) Case C.

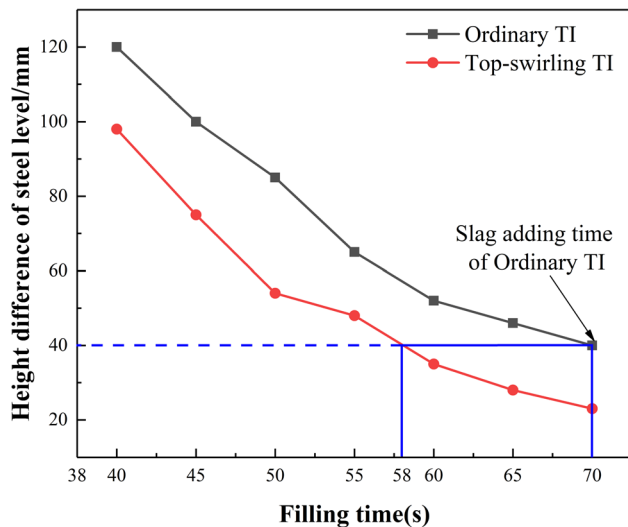


Fig. 8—Fluctuation of liquid level before slag addition in tundish with different TIs.

time of slag in the molten steel was 105 seconds, which was 85 seconds in Case B. During the slag adding, in the casting zone, the conditions of the tundish under different cases were basically same, and there would be no slag entrapment into the molten steel.

The reason for this phenomenon is that there is a large TKE region above TIs in Case B and Case C. When the molten steel returned to the free surface after entering the impact zone from LS, because the slag entrance was

upon the TIs, when the slag entered into the molten steel, the TKE offsets some kinetic energy of the slag, so that only a small amount of the slag entered the molten steel. In Case A, the molten steel from LS flowed upward along the tundish wall after reaching the bottom of the tundish. Without the offset of TKE of molten steel, a large amount of slag was entrapped into molten steel. In Case C, the molten steel would generate horizontal swirling flow under the action TS-TI, which could weaken part of kinetic energy of slag in the horizontal direction. Therefore, the slag floatation effect of Case C is superior to Case B.

Figure 10 shows the top view of variations of slag under different cases when the filling time is 72, 80, and 90 seconds, respectively. In Case B and Case C, in the casting zone, it took about 20 seconds from the beginning of slag adding to the steel surface is completely covering. After the slag completely covered the liquid level in the casting zone, the molten steel in the tundish was 11.7 t. However, in Case A, a stable molten steel exposed area would be formed after 25 seconds of slag adding, and the molten steel was completely covered after 150 seconds of slag adding. In Case A, the molten steel with a large TKE flowed to the casting zone from the impact zone, which hid the movement of slag spreading which in casting zone. Conversely, in Case B and Case C, the TKE of molten steel flow to the casting zone decreases under the action of TIs, and the flow to the casting zone was relatively slow, so that the slag could quickly cover the molten steel.

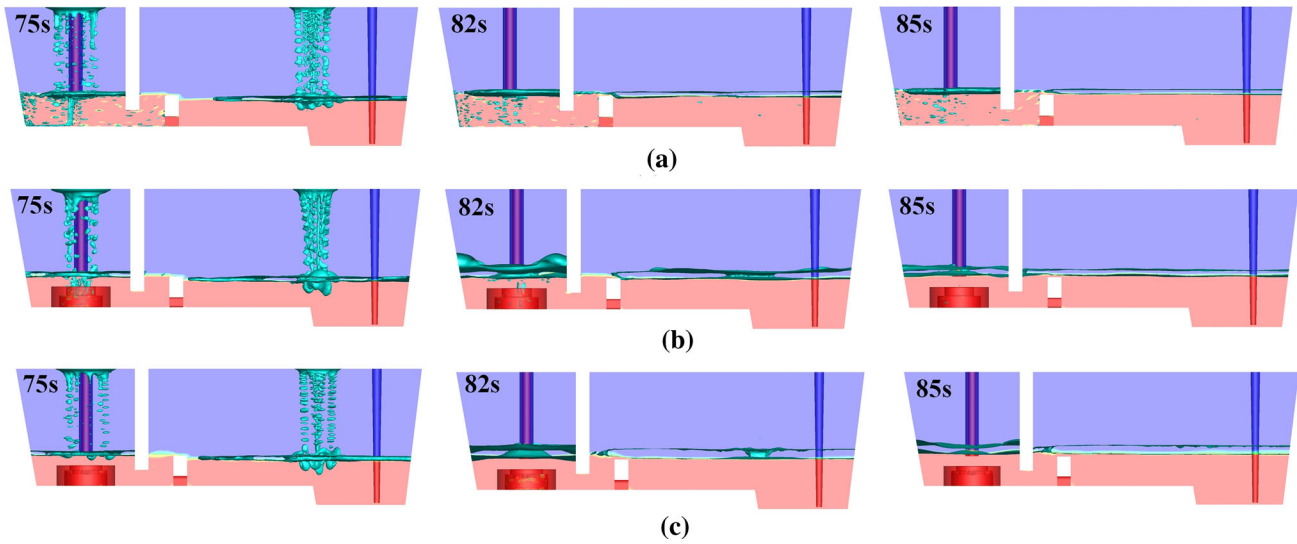


Fig. 9—Flow of steel slag in tundish during start-up: (a) Case A; (b) Case B; (c) Case C.

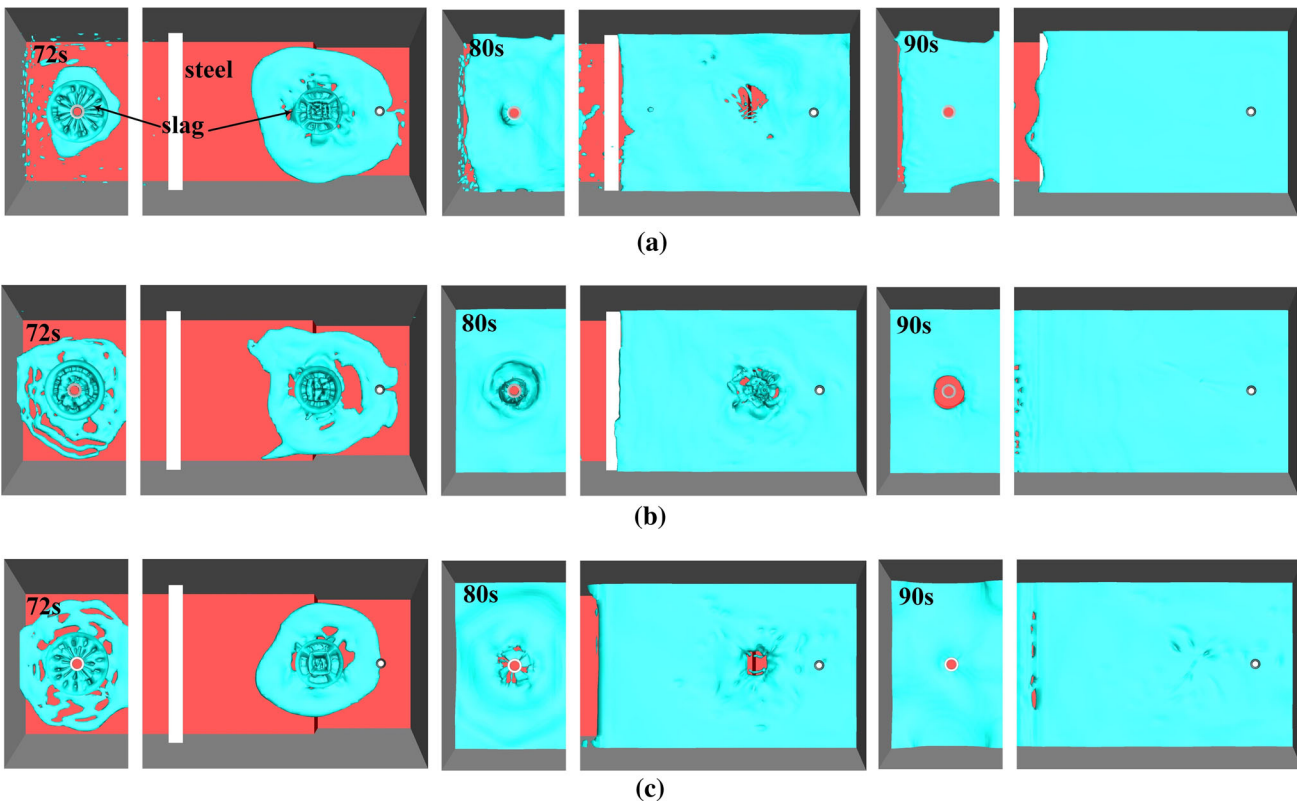


Fig. 10—Movement of slag during slag is added to tundish: (a) Case A; (b) Case B; (c) Case C.

C. Reoxidation Phenomenon

Figure 11 shows the exposure of molten steel with different TIs at filling time as 85, 95, 120, and 150 seconds, respectively. Due to the strong impact of upwelling flow and the shear force of horizontal flow, the slag layer is broken, which leads to the exposure of molten steel.

Figure 12 shows the variation of molten steel exposed area with time during the start-up operation. In Case A and Case B, the molten steel exposure would stabilize at about 1875 and 875 cm², respectively. While the steel exposure could be eliminated in Case C. Therefore, the TS-TI was beneficial to reduce the reoxidation and improve the quality of the casting billet during start-up operation.

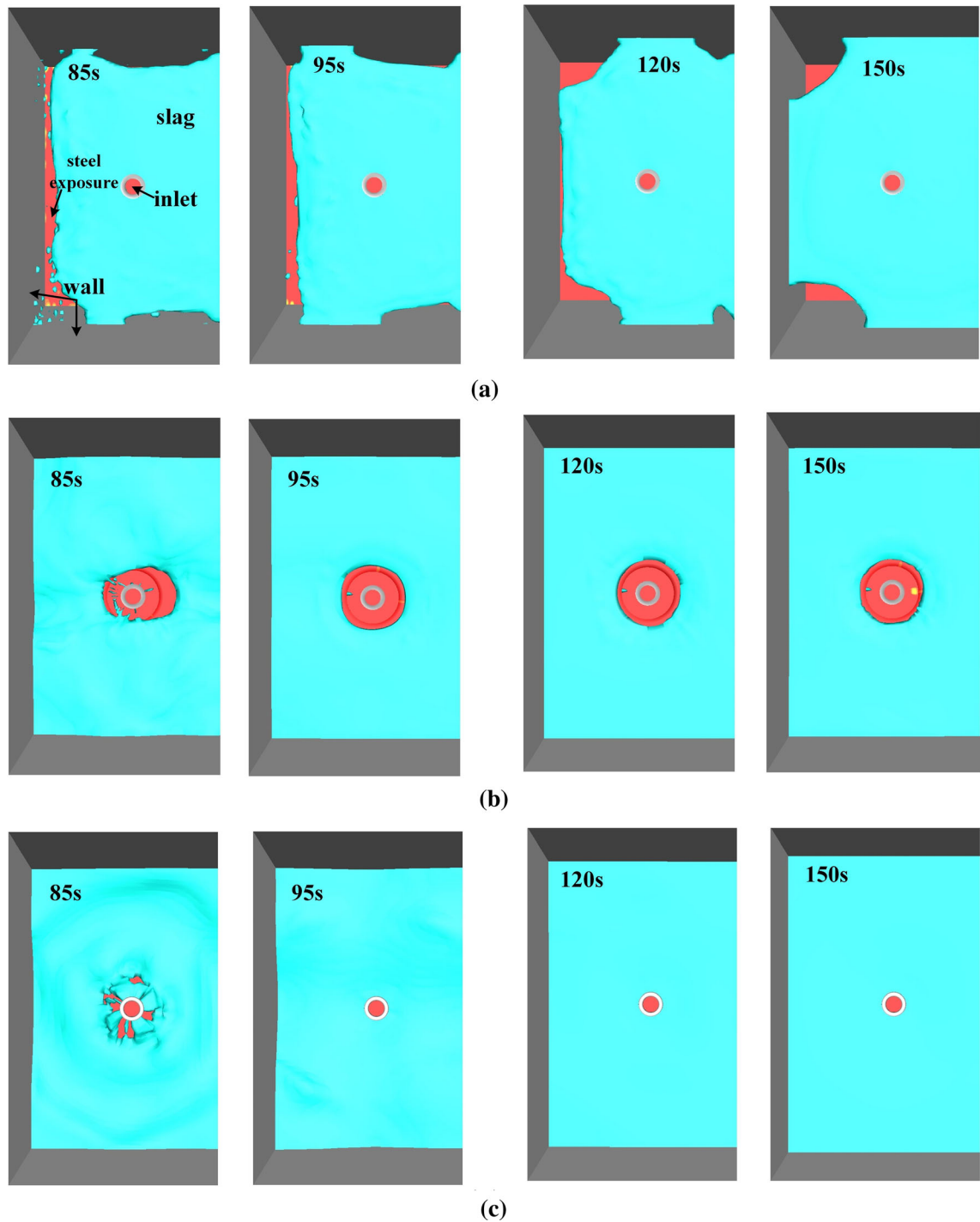


Fig. 11—Exposure of molten steel with different TIs at filling time are 85, 95, 120, and 150 s: (a) Case A; (b) Case B; (c) Case C.

Figure 13 shows the exposure of molten steel in the casting zone with different TIs at filling time as 85, 95, and 150 seconds, respectively. Figure 14 shows the variation of molten steel exposed area in casting zone with time during the start-up operation. The steel exposed area in the casting zone gradually decreased

until it completely covers the molten steel after slag adding. The slag completely covered the molten steel after 150 seconds in Case A, and in Case B and Case C, the slag completely covered the molten steel after 95 seconds.

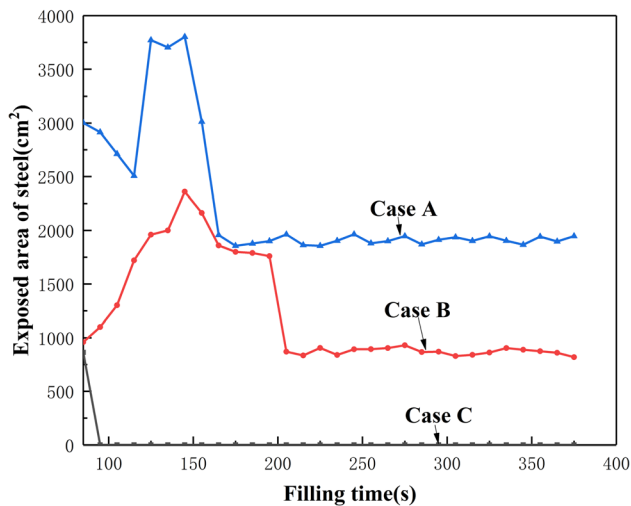


Fig. 12—Variation of steel exposed area in impact zone of the tundish with filling time under different TIs during start-up operation.

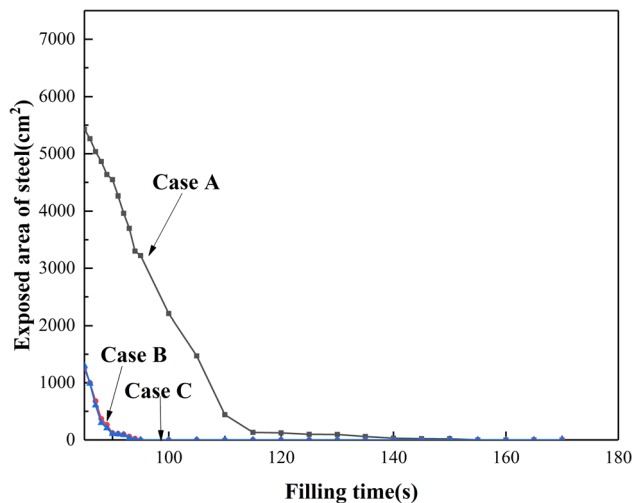


Fig. 14—Variation of steel exposed area in casting zone of the tundish with filling time under different TIs during start-up operation.

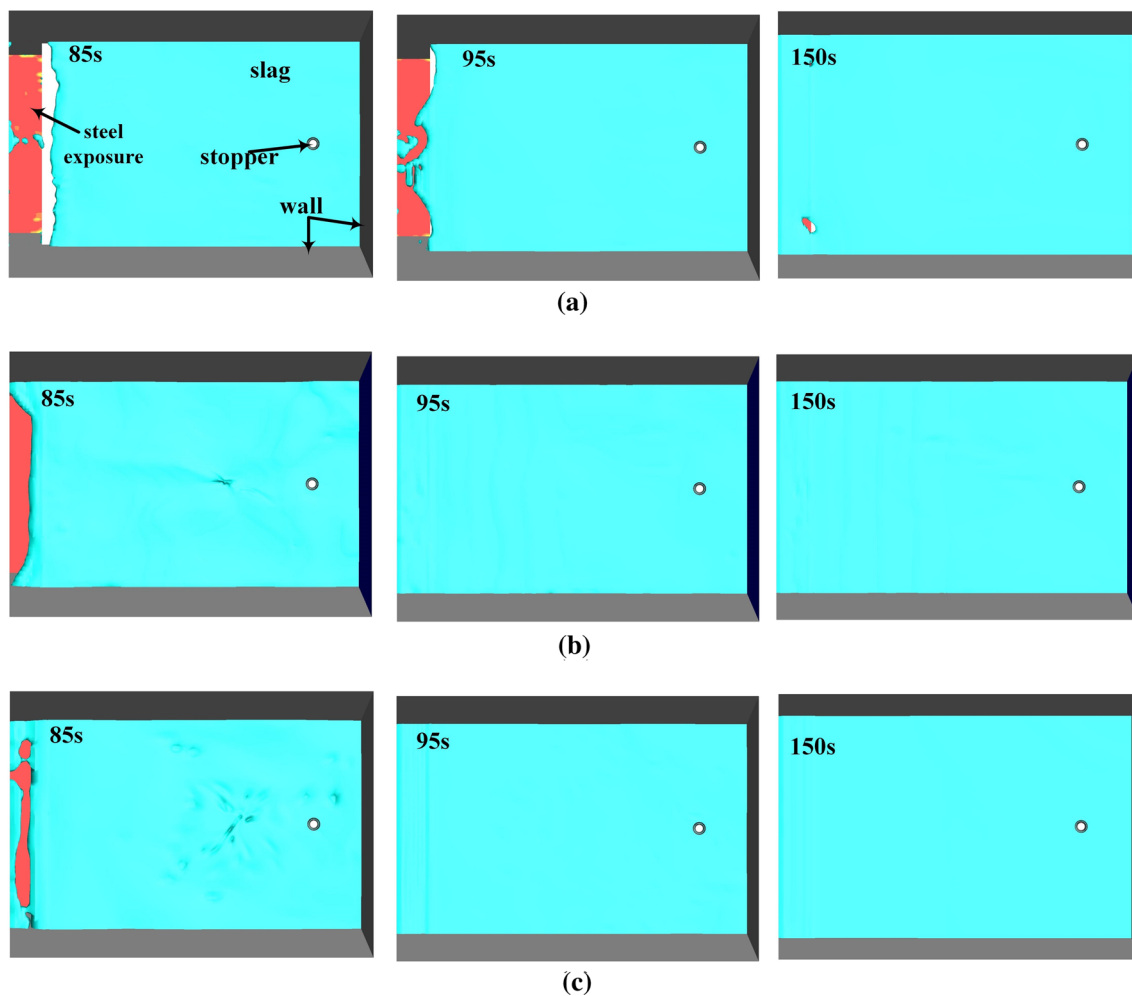


Fig. 13—Exposure of molten steel in the casting zone with different TIs at filling time are 85, 95, and 150 s: (a) Case A; (b) Case B; (c) Case C.

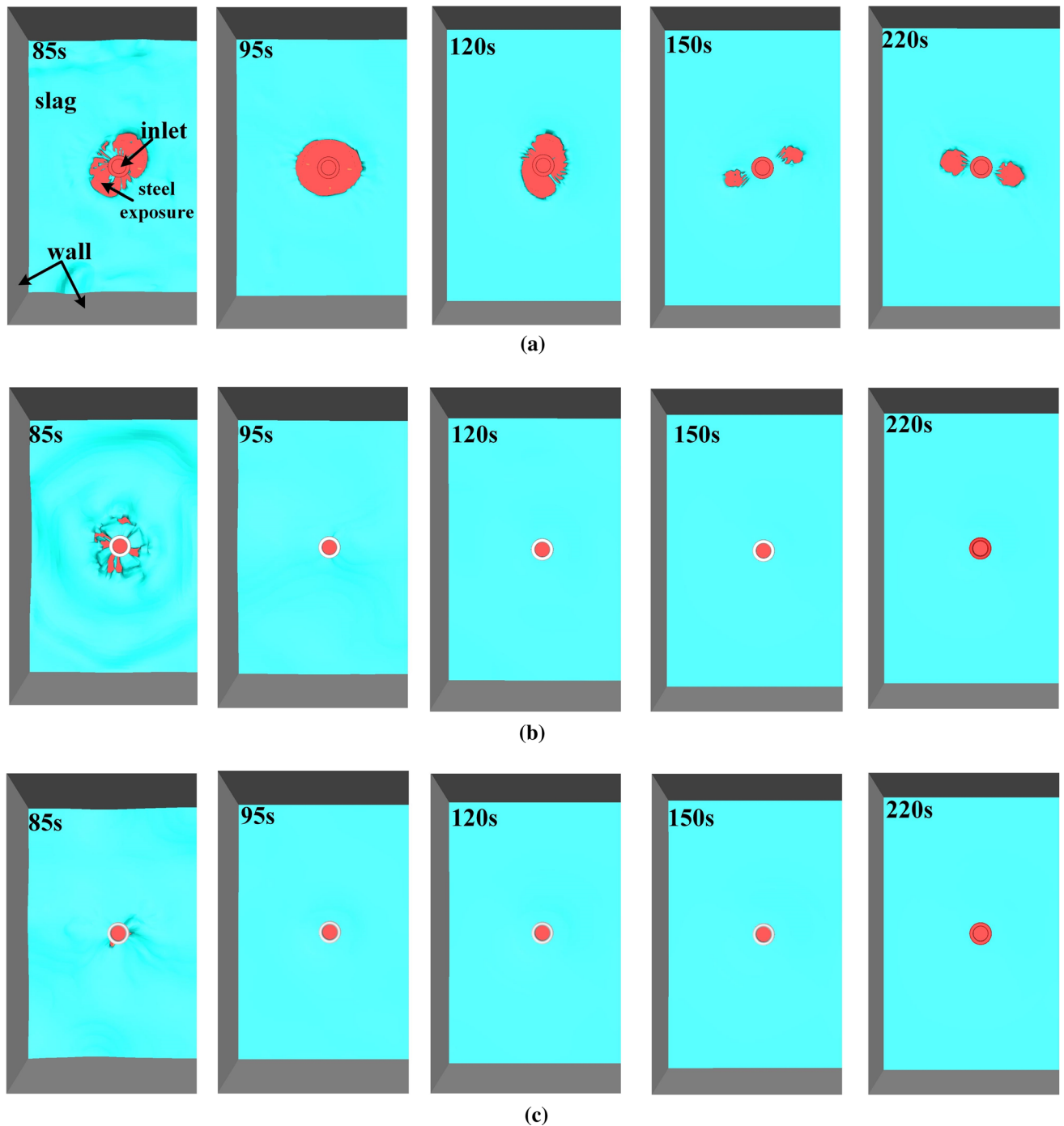


Fig. 15—Exposure of molten steel with different guide vane thickness at filling time are 85, 95, 120, 150, and 220 s: (a): 20 mm; (b): 40 mm; (c): 60 mm.

D. Effect of the Guide Vane Thickness

The thickness of the guide vane in a TS-TI is one of the most important parameters. When the thickness of the guide vane increases, it is easier to generate swirling flow, however, the erosion of molten steel on the guide vane will be more serious, the service life of the TI is shortened. Therefore, the thickness of the guide vane should be as short as possible on the premise of no steel

exposure during the start-up operation. In above study, the thickness of the guide vane was 40 mm, this section compares and analyzes the three phases of steel–slag–gas flow behavior during the start-up operation under a TS-TI with the guide vane thickness of 20, 40, and 60 mm, respectively. Figure 15 shows the distribution of the slag in the impact zone under the TS-TI with different thickness of guide vanes, and the filling times

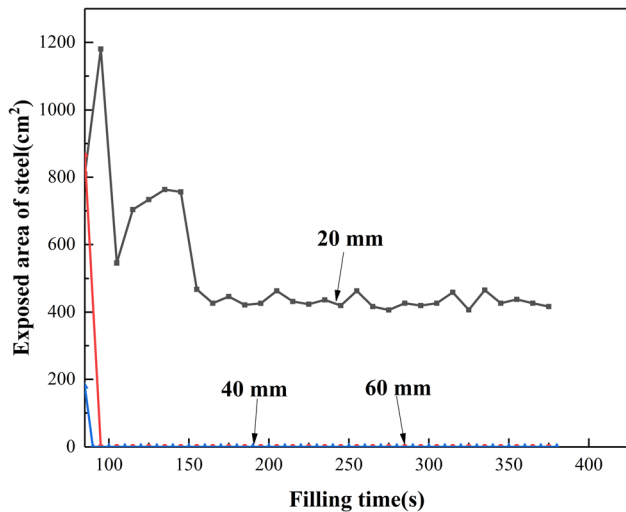


Fig. 16—Variation in exposed area with different TIs of different guide vane thickness during start-up operation.

are 85, 95, 120, 150, and 220 seconds, respectively. Figure 16 shows the variation in exposed area with filling time with different thickness of guide vanes during start-up operation.

After the slag adding process was completed and the molten steel was completely covered by the slag, when the thickness of the guide vane was 20 mm, the exposed molten steel would eventually stabilize at about 430 cm². No molten steel was exposed to air when the thickness of the guide vane were 40 and 60 mm. Indicating that when the thickness of the guide vane is greater than 40 mm, the expected goal can be achieved, so it is most suitable to use a guide vane with a thickness around 40 mm.

V. CONCLUSIONS

In this paper, the influence of TS-TI on the movement of steel–slag–gas during start-up operation was analyzed by mathematical model, and the advantages of TS-TI over without TI and ordinary TI were compared. The conclusions are summarized as follows:

- (1) In the numerical simulation and water model experiment, the error of exposed area in impact zone is less than 6 pct, and the error of average residence time of molten steel in tundish is less than 8 pct.
- (2) The tundish with a TS-TI can generate a swirling flow to reduce the average velocity and liquid level fluctuation of the tundish. At the same time, compared with an ordinary TI, the time of slag adding operation can be advanced by 11.5 seconds, which would conducive to improving production efficiency.
- (3) The tundish with a TS-TI can completely inhibit the exposure of molten steel, which will be beneficial to the cleanliness of steel. The exposure of molten steel after stabilization with an ordinary TI and the tundish without use the TI is stabilized at 875 and 1875 cm², respectively.

- (4) When the thickness of the guide vane is 20 mm, the molten steel exposure is stable at about 430 cm². When the thickness of the guide vane is 40 and 60 mm, the molten steel will not be exposed during the start-up operation.
- (5) By comprehensively consideration, a TS-TI with the guide thickness around 40 mm is most appropriate for optimization the multiphase flow behaviors in the current single-strand slab tundish during both steady-state and transient processes.

ACKNOWLEDGMENTS

The authors would like to express their gratitude for the financial support provided by the National Natural Science Foundation of China (52004191), the China Postdoctoral Science Foundation (2022M711120) and the Science and Technology Research Project of Education Department of Hubei Province (B2022020). Besides, the numerical calculation is supported by High-Performance Computing Center of Wuhan University of Science and Technology.

CONFLICT OF INTEREST

On behalf of all authors, the corresponding author states that there is no conflict of interest.

REFERENCES

1. B.G. Thomas: *Steel Res. Int.*, 2018, vol. 89, p. 1700312.
2. H. Tang, K. Wang, X. Li, J. Liu, and J. Zhang: *Metals*, 2021, vol. 11, p. 1075.
3. Y. Sahai: *Metall. Mater. Trans. B*, 2016, vol. 47B, pp. 2095–2106.
4. J. Zhang, Q. Liu, S. Yang, Z. Chen, J. Li, and Z. Jiang: *ISIJ Int.*, 2019, vol. 59, pp. 1167–77.
5. S. Basu, P.S. Devi, and H.S. Maiti: *J. Mater. Res.*, 2004, vol. 19, pp. 3162–71.
6. Y. Ueda, T. Nakajima, T. Ishii, R. Tsujino, and M. Iguchi: *High Temp. Mat. Pr-Isr.*, 2012, vol. 31, pp. 405–10.
7. D. Mazumdar: *Steel Res. Int.*, 2019, vol. 90, p. 1800279.
8. A. Cwudziński, J. Jowska, and B. Gajda: *Steel Res. Int.*, 2020, vol. 91, p. 2000027.
9. B.M. Braga and R.P. Tavares: *Metall. Res. Technol.*, 2018, vol. 115, p. 409.
10. S. Chakraborty and Y. Sahai: *Metall. Trans. B*, 1992, vol. 23B, pp. 153–67.
11. H. Zhang, J. Wang, Q. Fang, G. Wu, P. Zhao, and H. Ni: *Steel Res. Int.*, 2022, vol. 93, p. 2100536.
12. R.D. Morales, J. Guarneros, K. Chattopadhyay, A. Nájera-Bastida, and J. Rodriguez: *Metals*, 2019, vol. 9, p. 394.
13. R.D. Morales, J. Guarneros, A. Nájera-Bastida, and J. Rodriguez: *JOM*, 2018, vol. 70, pp. 2103–08.
14. S. López-Ramirez, J. Palafox-Ramos, R.D. Morales, J.D.J. Barreto, and D. Zacharias: *Metall. Mater. Trans. B*, 2001, vol. 32B, pp. 615–27.
15. R.D. Morales, S. Garcia-Hernandez, J.D.J. Barreto, A. Ceballos-Huerta, I. Calderon-Ramos, and E. Gutierrez: *Metall. Mater. Trans. B*, 2016, vol. 47B, pp. 2595–2606.
16. B. Yang, H. Lei, Q. Bi, J. Jiang, H. Zhang, Y. Zhao, and J. Zhou: *Steel Res. Int.*, 2018, vol. 89, p. 1800145.
17. W. Huang, S. Chang, Z. Zou, H. Song, Y. Qu, L. Shao, and B. Li: *ISIJ Int.*, 2022, vol. 62, pp. 1439–49.

18. P. Ni, M. Ersson, L.T.I. Jonsson, and P.G. Jönsson: *Metall. Mater. Trans. B*, 2018, vol. 49B, pp. 723–36.
19. ANSYS Fluent 15.0 *Theory Guide*, Southpointe, 2013.
20. Q. Fang, H. Zhang, J. Wang, C. Liu, and H. Ni: *Metall. Mater. Trans. B*, 2020, vol. 51B, pp. 1705–17.
21. H. Zhang, Q. Fang, R. Luo, C. Liu, Y. Wang, and H. Ni: *Metall. Mater. Trans. B*, 2019, vol. 50B, pp. 1461–75.
22. H. Zhang, C. Liu, Q. Fang, Y. Wang, H. Ni, and C. Liu: *Ironmak. Steelmak.*, 2020, vol. 47, pp. 1029–40.

Publisher's Note Springer Nature remains neutral with regard to jurisdictional claims in published maps and institutional affiliations.

Springer Nature or its licensor (e.g. a society or other partner) holds exclusive rights to this article under a publishing agreement with the author(s) or other rightsholder(s); author self-archiving of the accepted manuscript version of this article is solely governed by the terms of such publishing agreement and applicable law.